Journal of Materials Chemistry A

ROYAL SOCIETY OF CHEMISTRY

REVIEW

View Article Online
View Journal | View Issue

Cite this: J. Mater. Chem. A, 2022, 10, 19304

Low-temperature resistant gel polymer electrolytes for zinc–air batteries†

Jiao Wu,[ab] Yuchao Wang,[a] Danni Deng,[b] Yu Bai,[a] Mengjie Liu,[a] Xin Zhao,[a] Xiang Xiong[a] and Yongpeng Lei *[a]

The rapid development of wearable devices has put forward high requirements for stable, solid-state, flexible and even stretchable energy storage systems. Owing to their high specific energy density and volumetric energy density, metal–air batteries especially high-safety zinc–air batteries (ZABs), have attracted widespread attention. However, limited by the reduced ionic conductivity of electrolyte and the sluggish kinetics of oxygen reduction/evolution reactions at the air cathode during discharge/charge processes below 0 °C, the performances of ZABs severely deteriorate. Rationally designed gel polymer electrolytes (GPEs) not only offer superior mechanical performance but also provide ZABs with accelerated ion transport to boost electrochemical performance at low temperatures. Herein, the types of GPEs towards electrochemical energy systems are first summarized. And then, the research toolbox for GPEs and assembled ZABs is put forward. Next, the design strategies for low-temperature tolerant GPEs in ZABs are highlighted, such as introduction of organic solvents, alkalization of hydrogel electrolytes, construction of double-network electrolytes, *etc.* Finally, current challenges and perspectives are proposed. This review provides up-to-date insights on the rational design of GPEs for ZABs, which can be expanded to other metal–air batteries, metal–sulfur batteries, metal-ion batteries and so on.

Received 25th March 2022
Accepted 9th June 2022

DOI: 10.1039/d2ta02381d

rsc.li/materials-a

1. Introduction

The research studies on (quasi-) solid-state batteries used in flexible electronics have received great interest because of their portability, wearability, safety, *etc.*[1–3] At the same time, the demand for rechargeable batteries with high energy density under harsh conditions is increasing.[4] In particular, high latitudes/altitudes and other alpine regions place urgent requirements on batteries

[a]State Key Laboratory of Powder Metallurgy, Central South University, Changsha, Hunan, 410083, China. E-mail: leiyongpeng@csu.edu.cn; lypkd@163.com
[b]School of Material Science and Engineering, Central South University of Forestry and Technology, Changsha, Hunan, 410004, China

† Electronic supplementary information (ESI) available. See https://doi.org/10.1039/d2ta02381d

Jiao Wu received her Bachelor's degree from Dalian University (2020). She is currently pursuing her Master's degree.

Dr Yongpeng Lei received his BS degree (2003) and Master's degree (2006) from the National University of Defense Technology, and his PhD degree (2011) from the National University of Defense Technology with Prof. Yingde Wang. He started the study of functional nanomaterials in the Department of Chemistry, Tsinghua University in 2011, under the guidance of Acad. Yadong Li. He joined the faculty of the State Key Laboratory of Powder Metallurgy, Central South University in 2017 as a full professor.

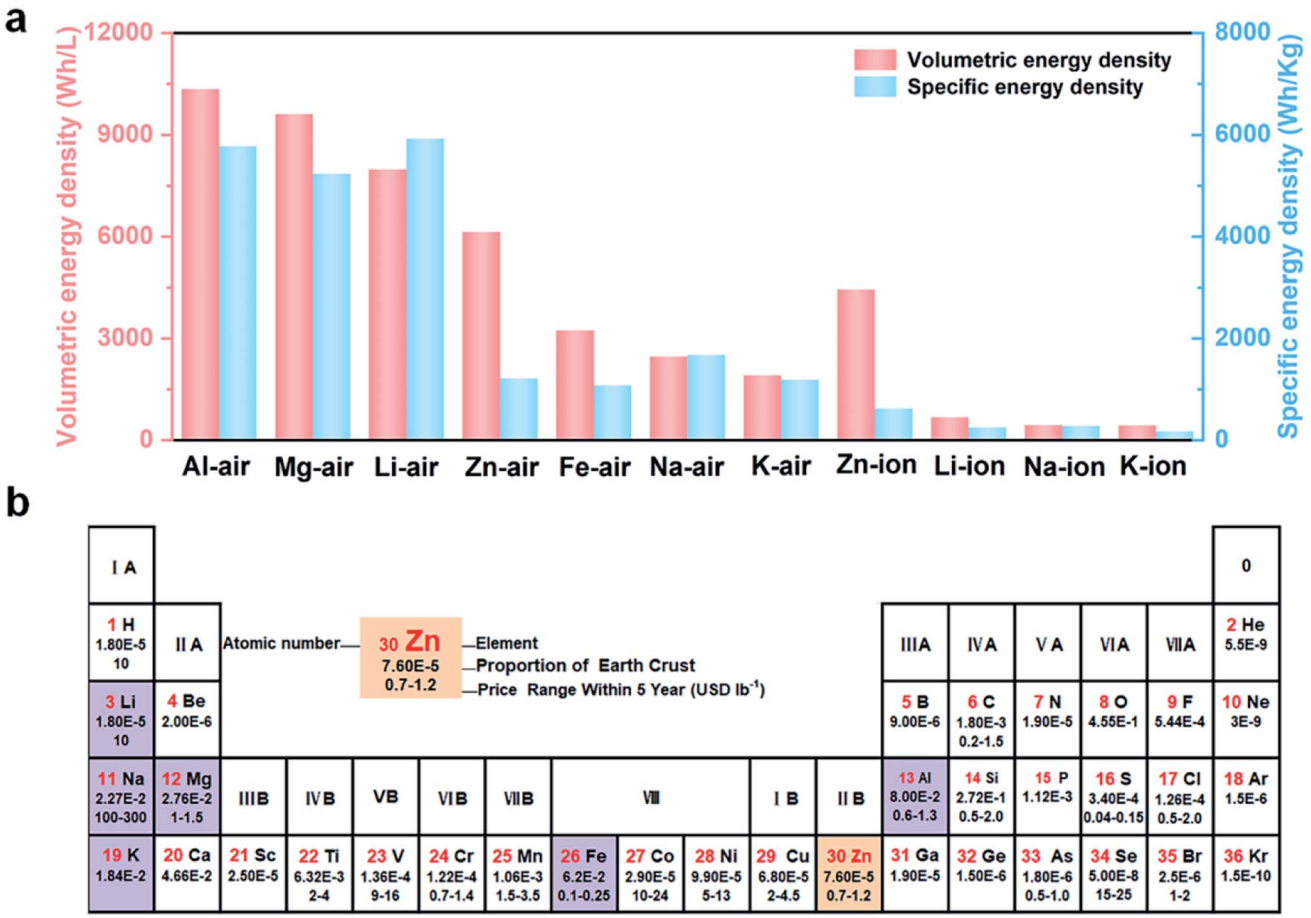

Fig. 1 (a) Comparison of energy density of typical metal–air batteries and metal-ion batteries. (b) The illustration of the abundance in the Earth's crust and price fluctuations of anode elements in metal–air batteries and metal-ion batteries.

with low-temperature resistance.[5,6] Owing to their significantly higher energy density than metal-ion batteries, metal–air batteries have attracted considerable attention as next-generation energy conversion/storage systems.[7,8] The theoretical specific energy density and volumetric energy density of typical metal–air batteries and metal-ion batteries are shown in Fig. 1a.[9,10]

Obviously, metal–air batteries with Mg, Al and Li anodes display higher theoretical energy densities than others. However, the high reactivity and low reduction potential of Mg/Al could result in rapid self-discharge and low coulombic efficiency of the corresponding metal–air batteries.[11] In addition, Li metal has a lower abundance in the Earth's crust and higher cost compared to other metal anode materials (Fig. 1b).[12] And it is easily damaged when exposed to air and electrolyte solutions, leading to potential safety hazards.[13] It's worth noting that metal Zn displays the intrinsic advantages of relatively high energy density, low cost, high safety (aqueous and non-flammable), *etc.*, which endow Zn–air batteries (ZABs) with broad prospects in advanced electronic devices.[14]

The timeline for the development of ZABs is shown in Fig. 2.[15–25] Since the emergence of ZABs, batteries have been continuously developed towards flexibility and low-temperature resistance. ZABs consist of a zinc anode, electrolyte and a porous air electrode with catalysts (Fig. 3a). Liquid electrolytes can be divided into alkaline, non-alkaline (neutral and acidic-alkaline dual electrolytes) and ionic liquid systems according to the pH and ion types.[26–29] In contrast to alkaline electrolytes, non-alkaline electrolytes face sluggish oxygen catalysis kinetics and low reactant concentrations while ionic liquids display relatively low conductivity and high cost, greatly limiting their applications in ZABs.[30] Therefore, most studies on ZABs have been carried out in alkaline electrolytes.[31,32] During the discharge process, the oxygen at the three-phase boundary among electrolyte, catalyst and air is reduced to hydroxide ions (OH^-): $O_2 + 2H_2O + 4e^- \rightarrow 4OH^-$ (oxygen reduction reaction, ORR). O_2 in air significantly reduces the cost, size and weight of the batteries. The generated OH^- ions migrate to the zinc electrode to form zincate ions ($Zn(OH)_4^{2-}$), which are further decomposed into insoluble zinc oxide (ZnO): $Zn + 4OH^- \rightarrow Zn(OH)_4^{2-} + 2e^-$, $Zn(OH)_4^{2-} \rightarrow ZnO + H_2O + 2OH^-$.[33] The whole discharge reaction is $2Zn + O_2 \rightarrow 2ZnO$. The charge process of ZABs is the opposite of the electrochemical reactions described above, and the oxygen evolution reaction (OER) occurs at the air electrode. At present, KOH solutions are widely used because of their high ionic conductivity (550 mS cm^{-1} for 35 wt% KOH solvent at 25 °C), low viscosity (2.2339 mPa s) and large oxygen

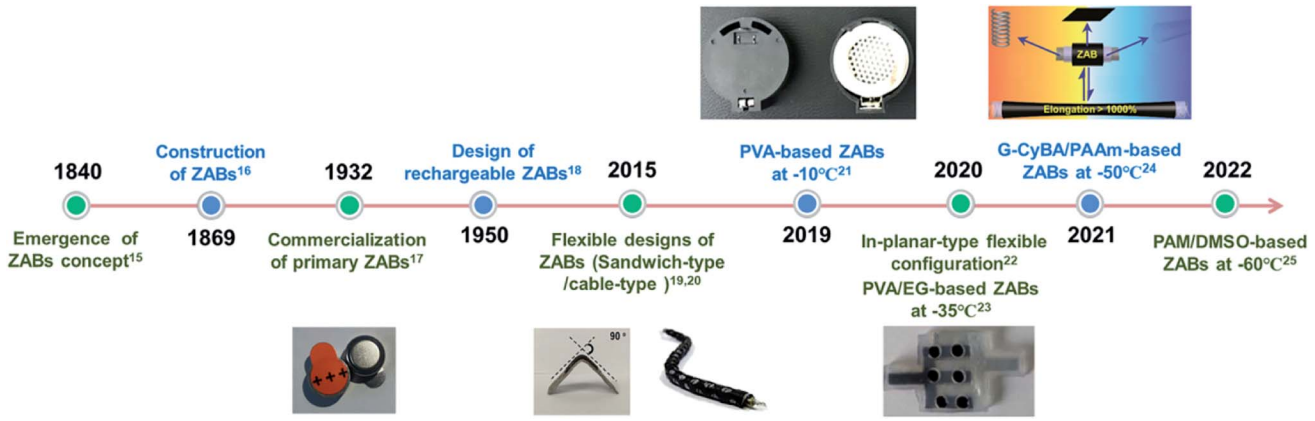

Fig. 2 Timeline for the development of ZABs.[15–25]

diffusion coefficient, offering outstanding electrochemical kinetics and mass transfer of batteries. At the same time, the salt solution of zinc is added into alkaline electrolyte to supply zinc ions and promote dissolution equilibrium.[34]

Up to now, the reported flexible ZABs are mainly based on three designs: sandwich-type,[19] cable-type[20] and in-plane-type (Fig. 3b–d).[22] In these battery configurations, to achieve ion conduction while separating the cathode/anode, some single-phase polymer backbones with alkaline (OH^-) functional groups (alkaline anion exchange membranes, AAEMs), alkaline electrolyte impregnated membranes (cellulose membranes or filter papers) and gel polymer electrolytes (GPEs) were developed.[35–37] However, the poor water retention properties of those membranes cause a rapid drop in ionic conductivity and an apparent attenuation in battery performance during long-term operation.[38] By contrast, GPEs possess a cross-linked network with a three-dimensional skeleton structure, which could hold a large amount of solvents to maintain a high ionic conductivity and provide great mechanical properties. Replacing liquid electrolytes with GPEs can not only meet the pursuit of portability and wearability, but also solve the problems of solvent volatilization and leakage to some extent.[39,40] In fact, GPEs play important roles as both electrolyte for ion migration and as a separator between the positive and negative electrodes, which significantly influence the power output, rate characteristics and cycle life of ZABs.[41,42]

Although there have been important breakthroughs in flexible ZABs at room temperature, their performance at low

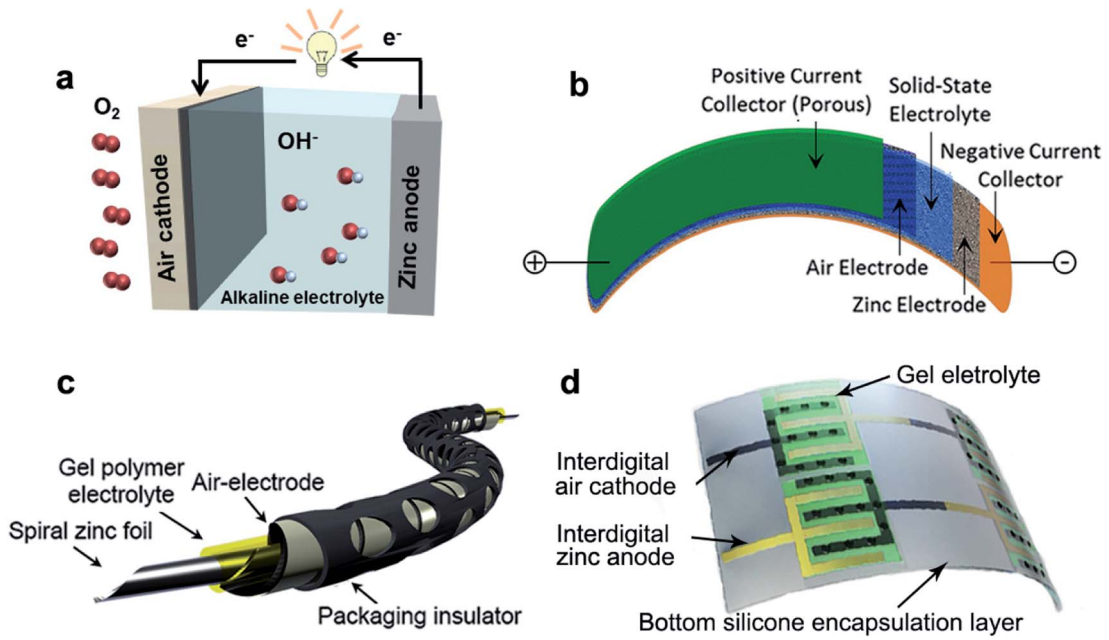

Fig. 3 Illustration of various configurations of ZABs: (a) liquid-type and (b) sandwich-type. Reproduced with permission from ref. 10. Copyright 2017, Wiley. (c) Cable-type. Reprinted with permission from ref. 20. Copyright 2015, Wiley. (d) In-plane-type. Reproduced with permission from ref. 22. Copyright 2020, Elsevier.

temperatures may be their Achilles' heel.[43] The freezing of GPEs causes a decrease in conductivity and an increment in internal resistance.[44] Modulating the solvated structure of electrolyte solutions has been proven to be a way to effectively improve the low-temperature tolerance of batteries.[45,46] However, GPEs with saturated alkaline electrolytes are far from meeting the requirements (high current density, long cycle, *etc.*) for extremely low-temperature scenarios (≤ -40 °C).[47–49] In addition, there is a lack of in-depth guidance for constructing low-temperature resistant GPEs.[50–52] In this review, the advantages, structures and working principles of ZABs are first introduced. Next, the commonly used polymers for advanced battery systems, especially ZABs are presented. And their characterization methods are systematically summarized in a research toolbox. Then, the design strategies (introduction of organic solvents, alkalization of hydrogel electrolytes and construction of double network (DN) hydrogel electrolytes) of low-temperature resistant GPEs towards ZABs are concluded in detail. The output performance, stability and mechanical properties of the assembled ZABs are also involved. Finally, the current challenges and prospects are presented.

2. The types and characterization methods of GPEs

In general, the ideal GPEs for ZABs should present the following properties: (i) High ionic conductivity. (ii) Excellent ionic accessibility and compatibility at the electrode/electrolyte interface. (iii) High chemical and electrochemical stability. (iv) Weak electrode corrosion. (v) Good thermal and mechanical stabilities under various climatic conditions. (vi) Easy packing and assembly. (vii) Low cost and environmental friendliness.[53] In practice, it is difficult for electrolytes to satisfy all requirements. To meet the applications in ZABs, the balance between different properties needs to be considered. Because of the great compatibility of the etheroxy group with various compounds, polyoxyethylene (PEO) was first studied as a solid polymer and used in all-solid-state electronic devices.[54] However, problems including low water absorption, poor interfacial properties and sharply decreased conductivity at high salt concentrations led to its gradual replacement by highly absorbent polymers, such as polyvinyl alcohol (PVA), polyacrylic acid (PAA), polyacrylamide (PAM), *etc.* To date, a variety of GPEs with specific characteristics have been applied to different battery systems (Table S1†). And the different types of monomers are summarized in Fig. 4. These GPEs contain abundant hydrophilic groups (–OH, –COOH, $-SO_3$, and $-NH_2$), which will facilitate fast polymerization and the accommodation of solvents.[55] To further improve the electrical conductivity, mass transfer capacity and flexibility of GPEs, strategies such as the introduction of additives and cross-linking are widely applied. What's more, complex functionality, *e.g.*, suppressing dendrites, frost resistance and self-healing could also be achieved. Therefore, the adjustable structural components of GPEs

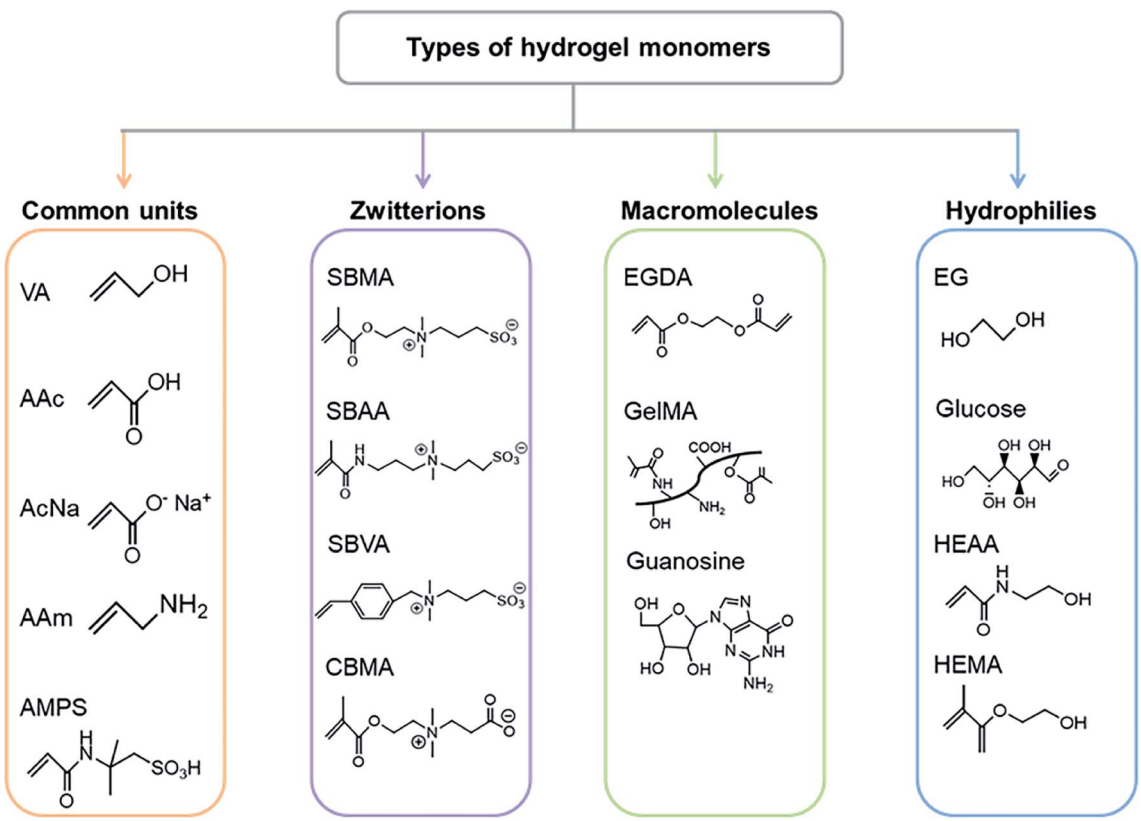

Fig. 4 Types of hydrogel monomers.

endow them with potential in flexible battery devices. The intrinsic properties of GPEs were clearly related to the output performance of assembled batteries. Considering the diversity and complexity of polymer monomers and additives, only three of the most commonly used polymers in ZABs are selected for introduction here.

PVA is a typical water-soluble polymer containing a large number of hydroxyl groups, which makes it easy to form macromolecular network structures through chemical cross-linking (Fig. 5a).[56] Therefore, this commonly used polymer has properties such as excellent chemical stability, durability, non-toxicity and a simple preparation process. The PVA-KOH-based GPEs are suitable for ZABs due to the above-mentioned advantages and their adaptability to KOH.[57–59] In 2000, Lewandowski and partners[60] prepared alkaline PVA GPE for the first time and investigated its electrochemical properties, which showed conductivities of 1 to 10 mS cm^{-1}. Cao *et al.*[61] fabricated PVA-KOH-based flexible electrolytes and assembled foldable ZABs, which exhibited a maximum power density of 28 mW cm^{-2}. After 30 cycles of repeated bending, the voltage overpotential (difference of charge–discharge potential) only increased to 30 mV. However, the tightly connected networks in PVA made it less absorptive to liquid electrolytes, which caused low ionic conductivity.[62] Through cross-linking,[63] heat treatment[64] and compounding with other materials,[65] the mechanical properties and absorption capacity of PVA can be enhanced.

PAA could form hydrogen bonds with lots of H_2O molecules on account of the existence of carboxylic acid groups, thus presenting strong water absorption and storage properties (Fig. 5b).[66] Compared to PVA, PAA demonstrates higher ionic conductivity and better mechanical properties.[67] PAA-KOH-based GPE was prepared by Iwakura *et al.*[68] in 2001. The strong alkali absorption capacity of PAA enables it to have high conductivity (600 mS cm^{-1}), similar to that of liquid electrolytes. However, the high water content also makes the PAA brittle, resulting in poor cycling performance of batteries. In view of this, the polyacrylic acid hydrogel electrolyte (sodium hydroxide neutralization in PAA, called PANa) was synthesized by Zhi and companions (Fig. 5c).[69] PANa has the following advantages: high chemical stability in strong alkaline electrolytes, super absorbence caused by the concentration difference of ionic groups inside and outside the hydrogel network, and robust mechanical properties even in high-concentration saturated solutions.[70,71] These strengths enable PANa-based ZABs to exhibit unprecedented ultra-long cycling stability (up to 800 cycles at 2 mA cm^{-2}). Meanwhile, due to the strong interactions between PANa and the zinc electrode, the stable electrolyte/

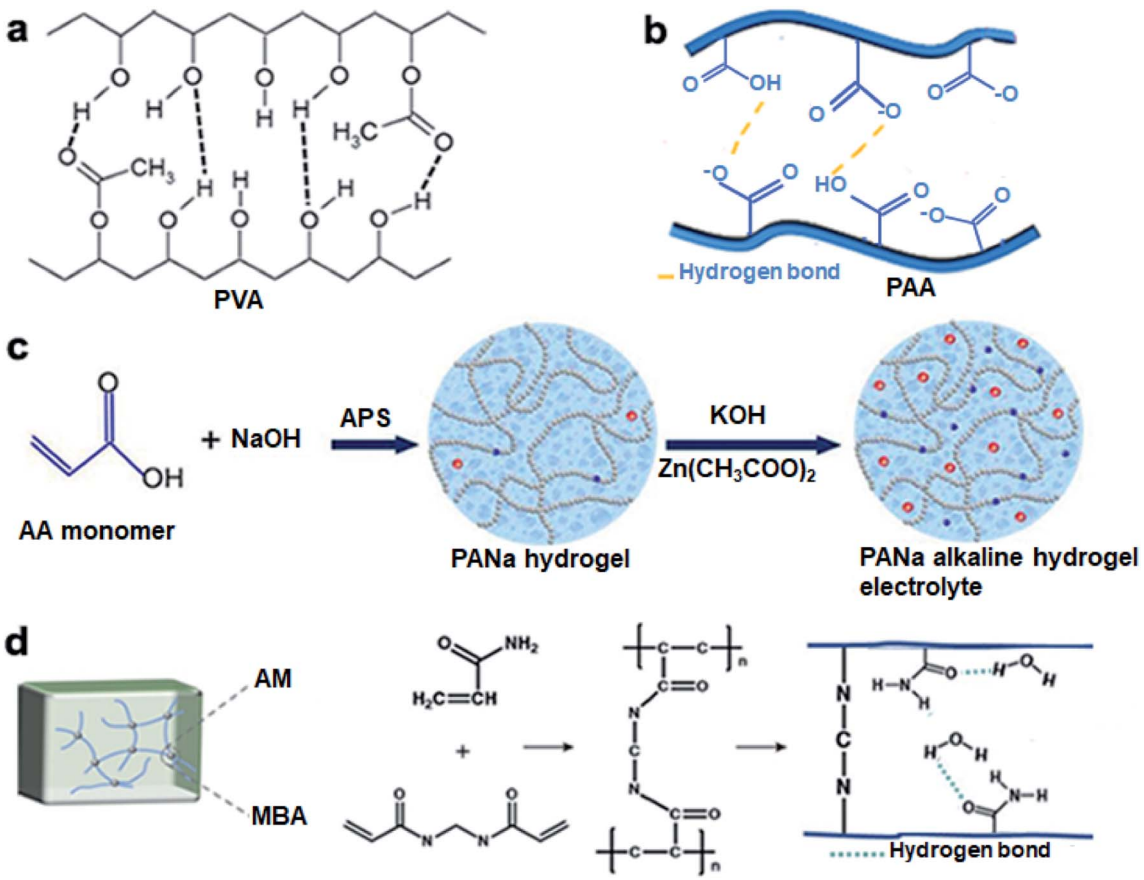

Fig. 5 Structures of (a) PVA and (b) PAA. Reproduced with permission from ref. 56. Copyright 2019, Elsevier. Reproduced with permission from ref. 66. Copyright 2020, Elsevier. The polymerization processes of (c) PANa and (d) PAM. Reproduced with permission from ref. 69. Copyright 2018, Elsevier. Reproduced with permission from ref. 72. Copyright 2022, Elsevier.

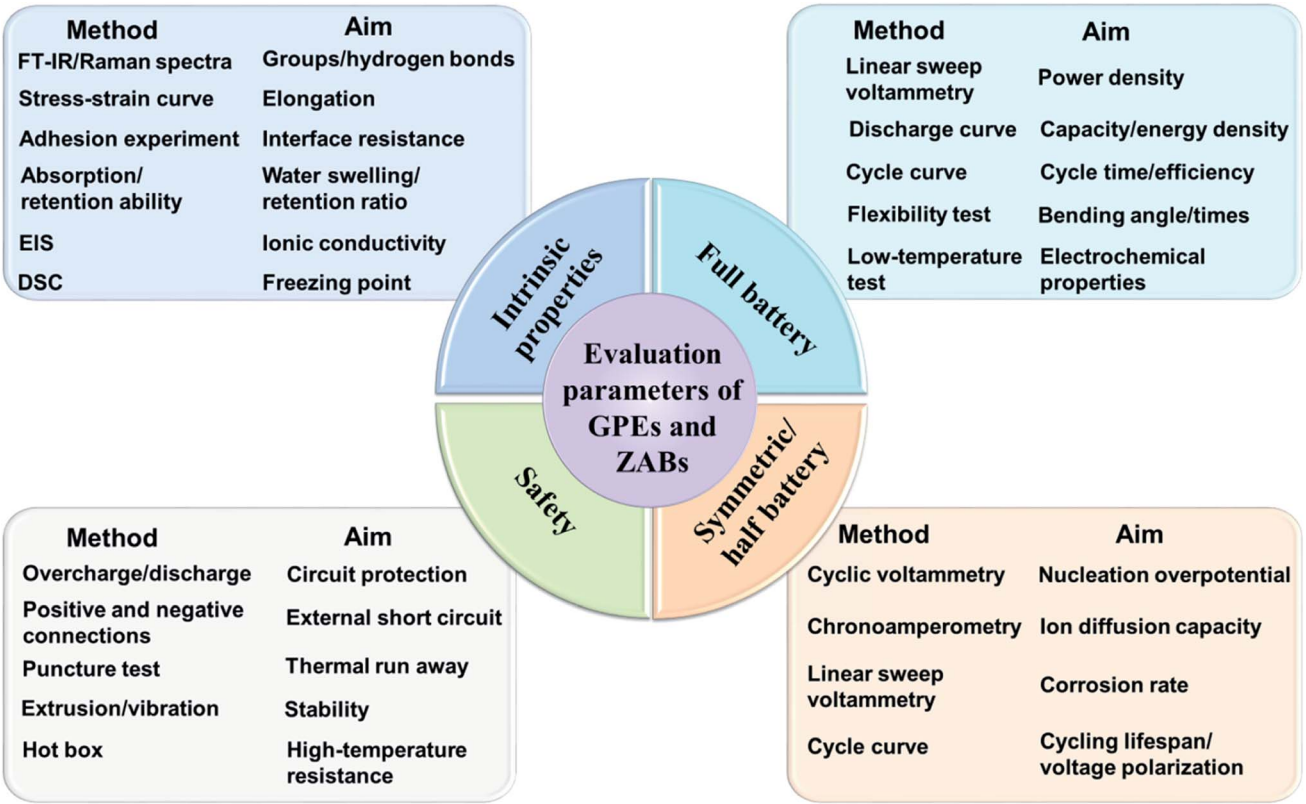

Fig. 6 Research toolbox of GPEs towards ZABs.

electrode interface was formed and the formation of zinc dendrites was mitigated.

PAM could easily form macromolecular networks by adding cross-linkers and initiators, of which the amide groups tend to form hydrogen bonds with water (Fig. 5d).[72] Owing to its sufficient water absorption capacity and excellent deformation ability, PAM is widely used in various battery systems.[73] In 2018, through *in situ* polymerization, Zhi *et al.*[74] prepared PAM alkaline hydrogel for ZABs. The hydrogen bond network in PAM could dissipate the externally applied energy. Even compressed to 54% of the deformation, the output power of PAM-based ZABs did not decrease obviously. During the 220 charge/discharge cycles, the discharge performance had almost no attenuation.

To study the physicochemical and mechanical properties of modified GPEs, the commonly used characterization methods are put forward and generalized in a toolbox (Fig. 6). For the intrinsic properties of GPEs, the paths of polymerization and cross-linking could be characterized using Fourier transform infrared (FT-IR) spectra and Raman spectra. Meanwhile, aiming at the applications in flexible ZABs, the mechanical properties, adhesion properties and water absorption/retention capacity of GPEs are fundamentally important parameters. Furthermore, under low-temperature conditions, the ion transport capacity (ionic conductivity) and the freezing point of GPEs can be estimated by electrochemical impedance spectroscopy (EIS) and differential scanning calorimetry (DSC), respectively. To verify the feasibility of GPEs in flexible ZABs, electrochemical tests are necessary to obtain various indicators of assembled batteries, such as: (i) Output performance, including power density, specific capacity and energy density. (ii) Cycle performance, including charge/discharge time and energy conversion efficiency. (iii) Flexibility performance, *e.g.* charge/discharge cycle at different bending angles or stress. (iv) Low temperature adaptability, performing those electrochemical tests at low temperatures. In addition, Zn||Zn symmetric cells and half reactions are generally used to assess the stability of the electrolyte/zinc interface. Such a simplified setup facilitates the detection of electrode polarization and corrosion. As another key issue, battery safety also needs to be considered, especially for wearable devices. Artificial over-charge/discharge, short-circuit, puncture experiments *etc*. deserve focus.

3. Design strategies for low-temperature tolerant GPEs in ZABs

The excellent water storage capacity provides the liquid-like properties of GPEs. However, the freezing of the water molecules in GPEs leads to the collapse of the internal network structure and loss of flexibility. At the same time, the decreased water solubility at low temperatures contributes to salt precipitates and a reduced ionic conductivity of the GPEs. Hence, the frost and low ionic conductivity of GPEs at low temperature are the main reasons for the degradation of battery performance.[75] On the one hand, the freezing GPE could not sufficiently come

into contact with the catalytic active sites, which results in large interfacial resistance, high overpotential and low current during battery operation.[76] On the other hand, the low ionic conductivity slows down the reaction kinetics, leading to severe polarizations and capacity degradation.[77] Considering the formation of ice crystals is an ordered arrangement of free H_2O molecules linked by hydrogen bonds, the suitability of GPEs for low temperatures needs to overcome the bonding between solvent molecules. The following three strategies have been applied: (1) The introduction of organic solvents, such as dimethyl sulfoxide (DMSO), ethylene glycol (EG), glycerol (Gly), *etc.*, to break the hydrogen bonds between free H_2O molecules. (2) The alkalization of hydrogels to enhance the binding energy between hydrogel networks and H_2O molecules to inhibit the presence of free water. (3) The design of DN GPEs to add hydrophilic backbones and reduce the freezing point. Freeze-resistant and compatible GPEs enable battery systems to adapt to extreme conditions.

3.1 Introduction of organic solvents

The low-temperature resistance of electrolytes is mainly related to overcoming the bonding between free H_2O molecules, *i.e.* breaking the hydrogen bonds. Many small molecule solvents containing hydrogen bonded acceptors or donors perform the function of lowering the freezing point, such as various alcohols and especially DMSO with a high donor number.[78,79] These organic solvents could serve as good media and form hydrogen bonds with free H_2O molecules, thus limiting the activity of water. Besides, several studies have demonstrated that the

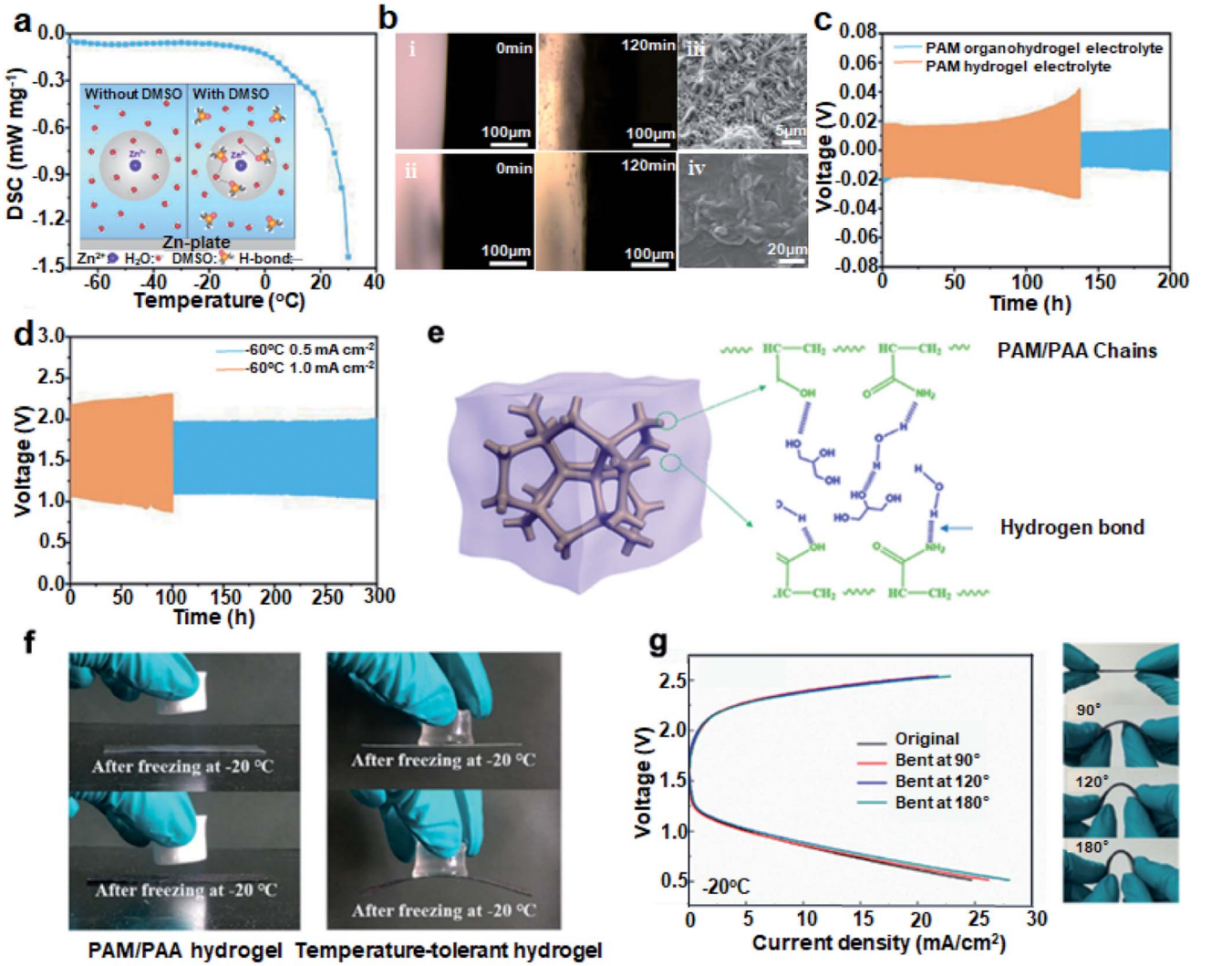

Fig. 7 (a) DSC curve of PAM organohydrogel electrolyte. The inset shows the schematic diagram of the effect of DMSO. (b) The *in situ* optical visualizations of the interface during charge/discharge at 5 mA cm^{-2} in (i) 6 M KOH + 0.2 M $Zn(Ac)_2$ and (ii) 6 M KOH + 0.2 M $Zn(Ac)_2$ + 2 M DMSO and SEM images of Zn plates after cycling with (iii) PAM hydrogels and (iv) PAM organohydrogels as electrolytes, respectively. (c) Cycling performance of symmetric Zn||Zn batteries at 2 mA cm^{-2}. (d) Charge/discharge curves of ZABs at 0.5 and 1 mA cm^{-2} at −60 °C. (e) Schematic diagram of PAM/PAA with Gly. (f) Adhesion of the PAM/PAA hydrogels and the temperature-tolerant hydrogels to zinc flakes and carbon cloth. (g) Bending tests and charge/discharge polarization curves at −20 °C. Reproduced with permission from ref. 90. Copyright 2020, American Chemical Society.

introduction of organic solvents into electrolytes could inhibit the passivation of Zn surfaces and promote uniform Zn dissolution/deposition.[80–82]

Inspired by these, we[25] introduced DMSO into PAM and obtained the low-temperature resistant PAM organohydrogel electrolyte. As shown in the inset of Fig. 7a, Zn^{2+} is surrounded by a stable solvation structure in the water-based electrolyte. The high dielectric constant of DMSO (47.2) indicates that the addition of DMSO can easily replace H_2O within the solvent sheath of Zn^{2+}, thus reconfiguring the solvent structure. As a result, the "O" atoms in DMSO could combine with the "H" atoms in the H_2O molecules to form stronger hydrogen bonds, breaking the order of H_2O molecules at low temperatures and dramatically decreasing the freezing point. The DSC curve in Fig. 7a shows that the PAM organohydrogel had excellent frost resistance with a freezing point below −70 °C.

During the electrodeposition process, Zn^{2+} ions form tight ion pairs ($[Zn(H_2O)_6]^{2+}$) with free H_2O molecules. The large numbers of active H_2O molecules at the electrolyte/anode interface are easily decomposed because the equilibrium potential of H_2O/H_2 is higher than that of Zn^{2+}/Zn, leading to the generation of zinc dendrites and the occurrence of various side reactions (hydrogen evolution reaction and corrosion).[83,84] The addition of organic solvent molecules in place of active water to modulate the solvation conformation around Zn^{2+} to $[Zn(H_2O)_x]^{2+}$ ($x < 6$) can effectively reduce the solvation energy, which inhibits dendrites/side reactions and increases the reversibility of the Zn ions.[85] *In situ* optical visualization revealed that the zinc/electrolyte interface with the addition of DMSO to liquid electrolyte remained smooth after charge/discharge cycles, while the interface without DMSO was uneven (photos of (i) and (ii) in Fig. 7b). This means that side reactions such as hydrogen evolution and corrosion have occurred at the zinc anode, causing the interface to change. The scanning electron microscopy (SEM) images are also recorded to show that PAM hydrogel based batteries generate dense zinc dendrites after cycling, while the PAM organohydrogel based batteries have dendrite-free interfaces ((iii) and (iv) in Fig. 7b). Owing to the stable, dendrite-free interface and antifreeze organohydrogel, the long stripping/plating cycle of a Zn‖Zn symmetric cell exceeds 200 h (Fig. 7c). Also, the PAM-based full ZABs with the addition of DMSO exhibited record-breaking cycle stability at −60 °C. The charge/discharge life was up to 300 h at a current density of 0.5 mA cm^{-2} with a capacity retention of 90% at −60 °C (Fig. 7d). Li *et al.*[86] also added DMSO to construct DN poly(2-acrylamido-2-methylpropanesulfonic acid) (PAMPS)/PAM, which exhibited high mechanical strength and good ionic conductivity. Moreover, the introduction of DMSO could change the path of the OER in ZABs and reduce the charge voltage to improve the energy efficiency. These advantages bring out the extensive applications of DMSO in antifreeze electrolytes.

The layer structure of montmorillonite (MMT) could promote ionic conductivity by creating a directional conductive channel, which has been demonstrated to enhance the stability of hydrogels.[87] We[88] prepared PAM/MMT organohydrogel electrolytes in a mixed solution of DMSO and H_2O. The assembled PAM/MMT-based ZABs provided a maximum power density of 30 mW cm^{-2} at −40 °C, while maintaining an 86% specific capacity corresponding to ZABs at room temperature. This work provides a feasible way to improve the electrical conductivity of GPEs and the electrochemical properties of ZABs.

EG and Gly are also commonly used organic solvents with abundant hydroxyl groups. The strong hydrogen bond interactions between EG and H_2O molecules significantly weaken the hydrogen bond formation within the H_2O molecules, resulting in a low freezing point.[89] Xu *et al.*[90] introduced Gly into PAM/PAA hydrogels to investigate its effect on freezing behavior, adhesion and mechanical properties. As seen in Fig. 7e, the terminal groups on the PAM/PAA chains formed a large number of hydrogen bonds with Gly and H_2O molecules, which widened the operating temperature range to −20 to 70 °C. The Gly-free PAM/PAA hydrogels were frozen at −20 °C, while the temperature-tolerant hydrogels were almost unchanged. They remained tightly attached to the zinc anode and air electrode, reducing the interfacial internal resistance under bending (Fig. 7f). The discharge polarization curves of ZABs at different bending angles basically overlapped, which showed a high interfacial stability (Fig. 7g). In addition, Xi and partners[23] assembled the ZABs using PVA/EG that exhibited an open-circuit voltage of 1.25 V at −30 °C. The PVA/EG GPEs displayed frost resistance at −30 °C and high water retention at 70 °C. The usage of small-amount but efficient electrolyte additives greatly satisfies the requirements for low-temperature GPEs.

The introduction of small molecule organic additives containing hydrogen bond acceptors or donors is known to reduce the freezing point, but implies the partial sacrifice of ionic conductivity.[91] Moreover, the organic solvent molecules may impair the ORR/OER kinetics of ZABs, *i.e.* the reaction path changed from the expected oxygen catalysis reaction to an alcohol oxidation reaction after the addition of Gly solvent.[92] And the occurrence of side reactions greatly slows down the discharge rate of ZABs. Therefore, developing GPEs with high ionic conductivity and suppressing side reactions needs to be considered.

3.2 Alkalization of hydrogel electrolytes

The key factor affecting the freezing resistance of hydrogels is the polarity of their terminal groups. The more polar terminal groups in hydrogels, the stronger the interactions between hydrogels and H_2O molecules. The abundant polar groups help to anchor the free H_2O molecules in hydrogels, and this strong interfacial interaction could disrupt the ordered structure of H_2O molecules and inhibit the formation of ice crystals.[93] Alkalization of hydrogel electrolytes provides an effective strategy to enhance their polarity, which endows the electrolytes with both high ionic conductivity and excellent low-temperature resistance.

Thus, Chen *et al.*[94] proposed a carboxyl-alkalified PAA (A-PAA) electrolyte, and this strategy introduced a strong electrostatic attraction to generate more polarized terminal groups in hydrogels. Compared to the interactions between PAA and H_2O molecules (PAA–W), the interaction energy between A-PAA and

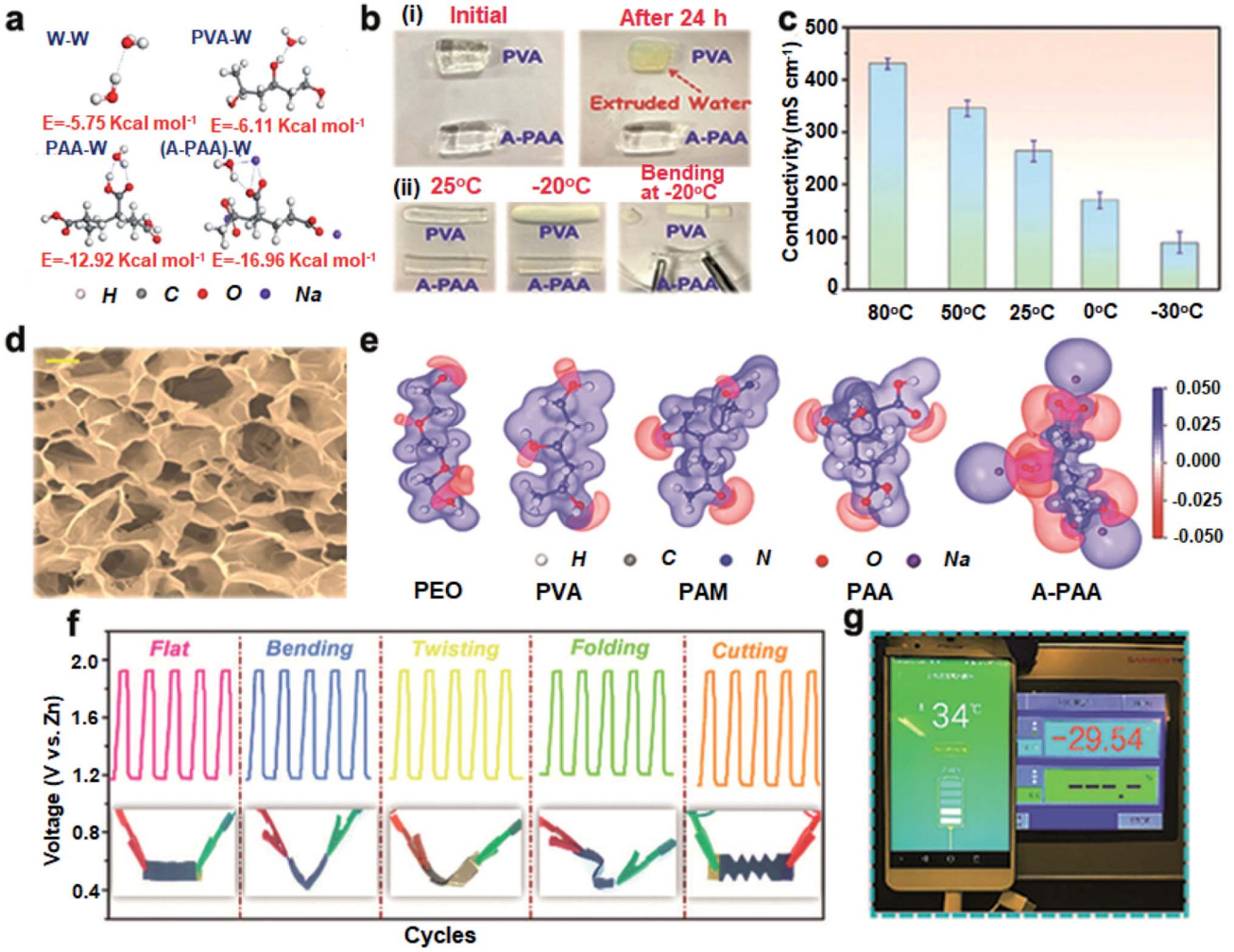

Fig. 8 (a) The interaction energy of W–W, PVA–W, PAA–W and (A-PAA)–W. (b) The comparison of the (i) water retention and (ii) frost resistance of the two hydrogels. Reproduced with permission from ref. 94. Copyright 2020, Wiley. (c) Ionic conductivity of KOH-filled A-PAA at different temperatures. (d) SEM image of the freeze-dried A-PAA hydrogels. Scale bar: 10 μm. (e) Electrostatic potential maps of H_2O molecules and different polymers. (f) Cycle curves of flexible ZABs under various mechanical deformations at −30 °C. (g) Photo of A-PAA-based ZAB charged phones at −30 °C. Reproduced with permission from ref. 95. Copyright 2021, the Royal Society of Chemistry.

H_2O molecules ((A-PAA)–W) significantly increased from −12.92 to −16.96 kcal mol^{-1}, which was also almost three times greater than that between two H_2O molecules (W–W) of −5.75 kcal mol^{-1} (Fig. 8a). As can be seen in Fig. 8b, the strong interactions with H_2O molecules made A-PAA unsusceptible to loss of water at room temperature and lowered the freezing point below −20 °C. In the following work, they combined the interface engineering of a stereoscopic electrode to greatly extend the operating temperature domain (−30 to 80 °C) of A-PAA-based batteries, with the high ionic conductivity of A-PAA (90 mS cm^{-1}) at −30 °C (Fig. 8c).[95] The ultra-high ionic conductivity of A-PAA hydrogels was further confirmed by the abundant interconnected pores that could adsorb large amounts of electrolytes and promote free diffusion of ions (Fig. 8d). The electrostatic potential maps of the different polymer backbones also verified the stronger attraction of A-PAA to H_2O molecules (Fig. 8e). Even at −30 °C, the power density of A-PAA-based ZABs reaches 63.6 mW cm^{-2}. And the energy density is 789 W h Kg^{-1}, which is 88.6% of that at room temperature. When performing charge/discharge cycles, it can continuously operate for up to 500 cycles (90 h). Benefiting from the good frost resistance and mechanical properties of A-PAA, the assembled ZABs maintained charge/discharge stability under bending, twisting, folding and cutting at −30 °C (Fig. 8f). Under this extreme condition, the ZABs could even charge the phone (Fig. 8g). These studies help in deeply understanding the interactions between hydrogel end groups and H_2O molecules, illustrating reasonable guidance for the exploration of freeze-tolerance mechanisms and the selection of suitable hydrogel matrices.

3.3 Construction of DN electrolytes

In addition to overcoming the mechanical bottleneck of single network (SN) hydrogels, the DN hydrogels consisting of two intertwined cross-linked networks also introduce more hydrophilic backbones to enhance the interactions between

hydrogels and H_2O molecules. The reversible toughening mechanism of DN hydrogel is based on the sacrificial bonds (and/or non-covalent bonds) and the ordered unfolding of the hydrogel network structure. And the increase of polar end groups simultaneously enhances the ability to bind with H_2O molecules, lowering the freezing point.[96] Thus, the construction of DN hydrogels provides attractive properties for various applications, such as toughness, mechanical strength, low-temperature resistance, *etc.*

For the needs of wide-temperature tolerance and high stretchability, the small molecule-based supramolecular-polymer (SP) DN hydrogel electrolytes consisting of guanosine-cyclohexylboronic acid (G-CyBA) networks interpenetrated with polyacrylamide (PAAm) networks were designed by Liu *et al.*[24] During the polymerization process, the G-CyBA monomers formed a stable hydrogen-bonded g-quadruplex structure through self-assembly. Then, π–π stacking of g-quadruplex formed the g-quadruplex nanowires with a highly ordered and right-handed helical superstructure (Fig. 9a). The apparent upfield shift of the B signal in the ^{11}B nuclear magnetic resonance spectra demonstrated the generation of G-CyBA borate complexes, which reveal the hierarchical assembly process of small molecule-based supramolecular polymer hydrogels (Fig. 9b). DSC curves showed that 6 M KOH-filled G-CyBA/PAAm SP DN hydrogels exhibited the melting peak of ice crystals at a lower temperature (−55.5 °C) compared to 6 M KOH-filled PAAm SN hydrogels (−43.3 °C) and 6 M KOH (−36.3 °C) (Fig. 9c). Simultaneously, the interaction energy between SP-DN $(G\text{-}CyBA)_4\text{-}K^+$/PAAm and H_2O molecules was significantly reduced to −26.32 kcal mol^{-1} with respect to the SN of PAAm (−3.02 kcal mol^{-1}) and the supramolecular $(G\text{-}CyBA)_4\text{-}K^+$ (−13.11 kcal mol^{-1}). Hence, SP-DN hydrogels presented excellent anti-freezing and anti-drying properties in the temperature range of −80 to 100 °C without impairing conductivity. As shown in Fig. 9d, the 6 M KOH-filled SP DN hydrogels provided an ionic conductivity of 300.1, 252.2 and 63.2 mS cm^{-1} at −40, −50 and −80 °C, respectively. They could also retain an elongation of over 1000% in a wide temperature range from −80 to 100 °C (Fig. 9e). Correspondingly, the assembled stretchable fibrous ZABs presented a power density of 107.6 mW cm^{-2} (Fig. 9f) and a charge/discharge cycle (2 mA cm^{-2}) over 48 h at −40 °C. In the *in situ* constant current discharge/charge test (2 mA cm^{-2}) ZABs immersed in water maintained stability for 2 h, which revealed their environmental stability (Fig. 9g). In

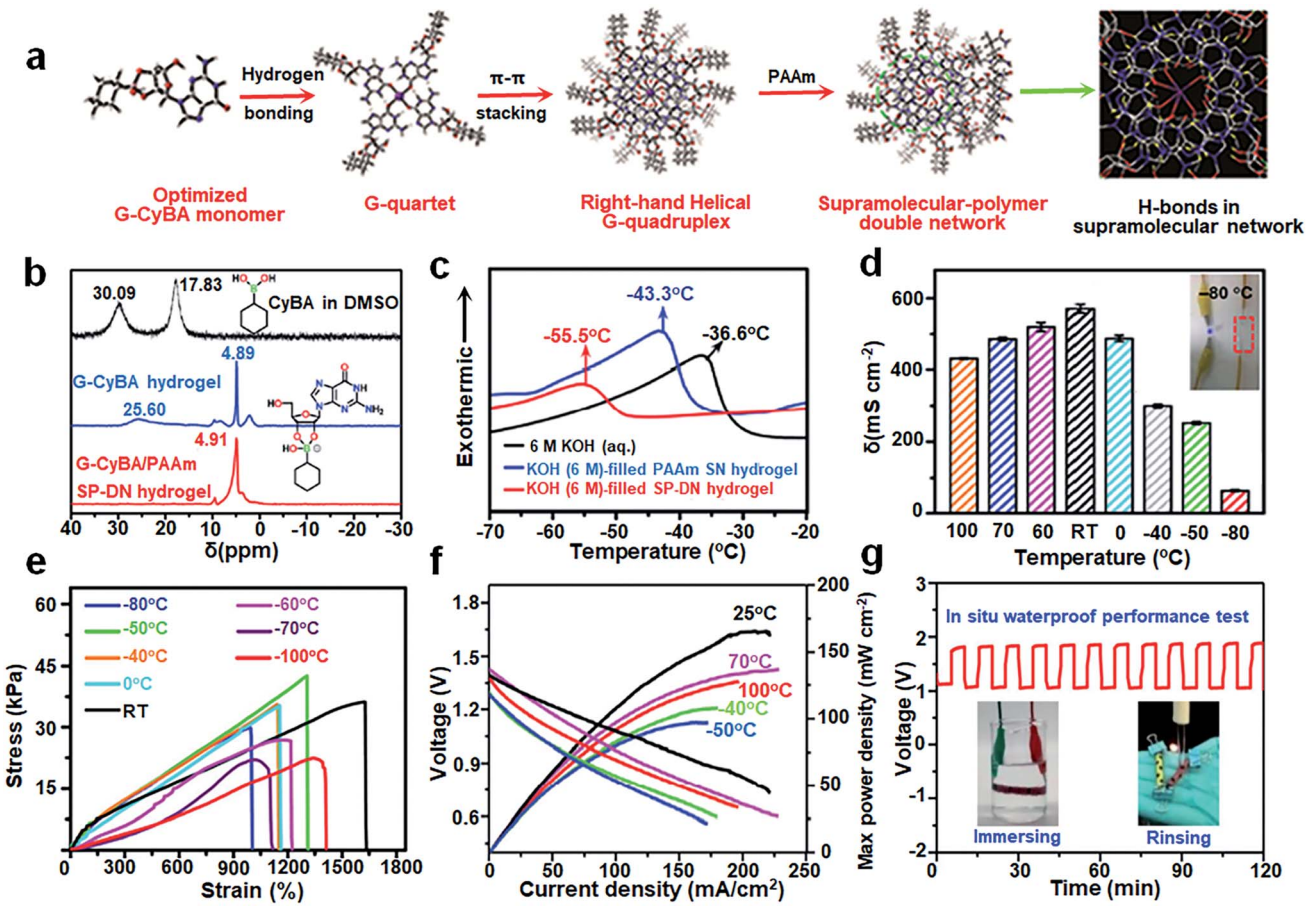

Fig. 9 (a) The assembly mechanism of the G-CyBA/PAAm SP-DN hydrogels. (b) ^{11}B nuclear magnetic resonance spectra (c) DSC curves of 6 M KOH filled G-CyBA/PAAm SP-DN hydrogel, 6 M KOH filled PAAm SN hydrogel and 6 M KOH. (d) Ionic conductivity and (e) tensile stress–strain curves of the SP-DN hydrogels at different temperatures. (f) Discharge curves and the corresponding power densities of the ZABs at various temperatures. (g) *In situ* waterproof performance test. Reproduced with permission from ref. 24. Copyright 2021, Elsevier.

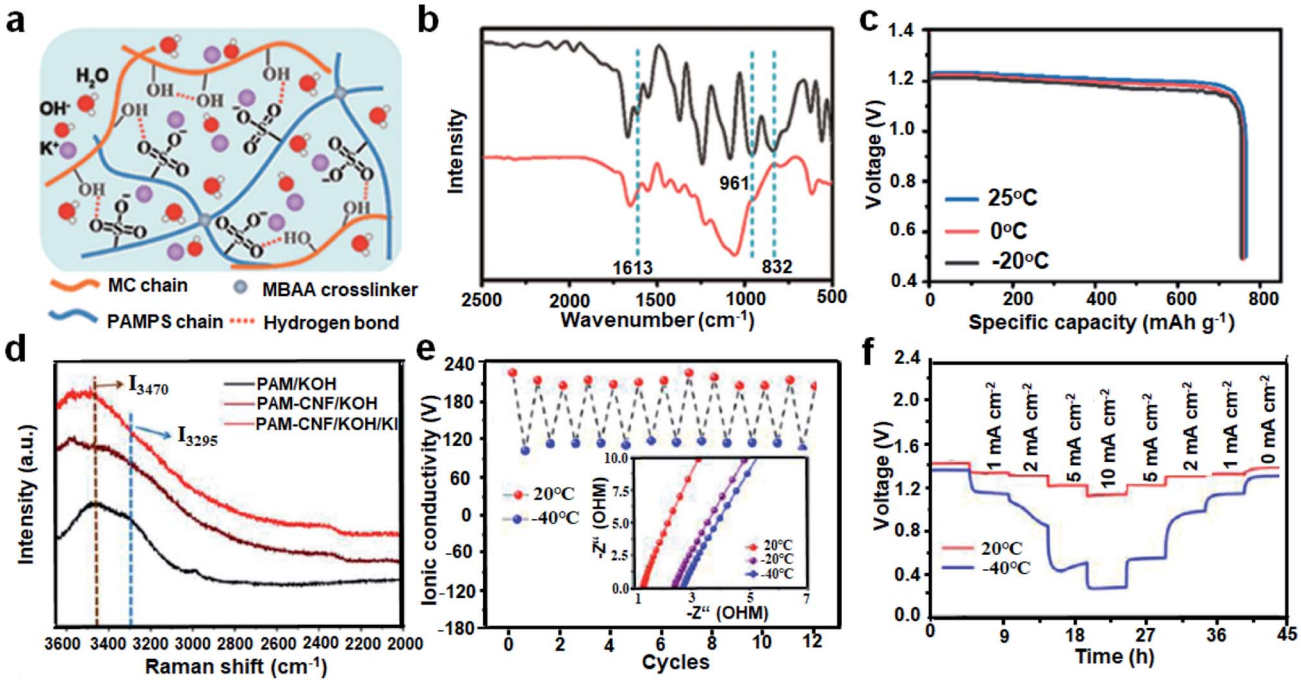

Fig. 10 (a) Schematic diagram of the PAMPS-K/MC hydrogels. (b) FT-IR spectra of the freeze-dried PAMPS/MC hydrogels (red) and the mixture of AMPS/MC (black). (c) Specific capacity of the ZABs at different temperatures. Reproduced with permission from ref. 97. Copyright 2021, American Chemical Society. (d) Raman spectra. (e) Ionic conductivity at 20 and −40 °C. (f) Rate performance. Reproduced with permission from ref. 101. Copyright 2021, Elsevier.

conclusion, the DN design of the hydrogel electrolytes with wide-temperature tolerance and flexibility offers options for environmental adaptability-required energy storage devices.

In order to efficiently combine superior mechanical properties, good ionic conductivity and antifreeze properties, Zheng *et al.*[97] prepared an alkaline DN hydrogel electrolyte (PAMPS-K/MC) interpenetrated by PAMPS and modified cellulose (MC) (Fig. 10a). From the FT-IR spectra of hydrogels before and after thermal polymerization, the vanishing of the characteristic peaks of AMPS at 1613, 961 and 832 cm^{-1} proves the covalent cross-linking of the PAMPS-K networks with MC (Fig. 10b). The generated hydrogen bonds will strongly enhance the

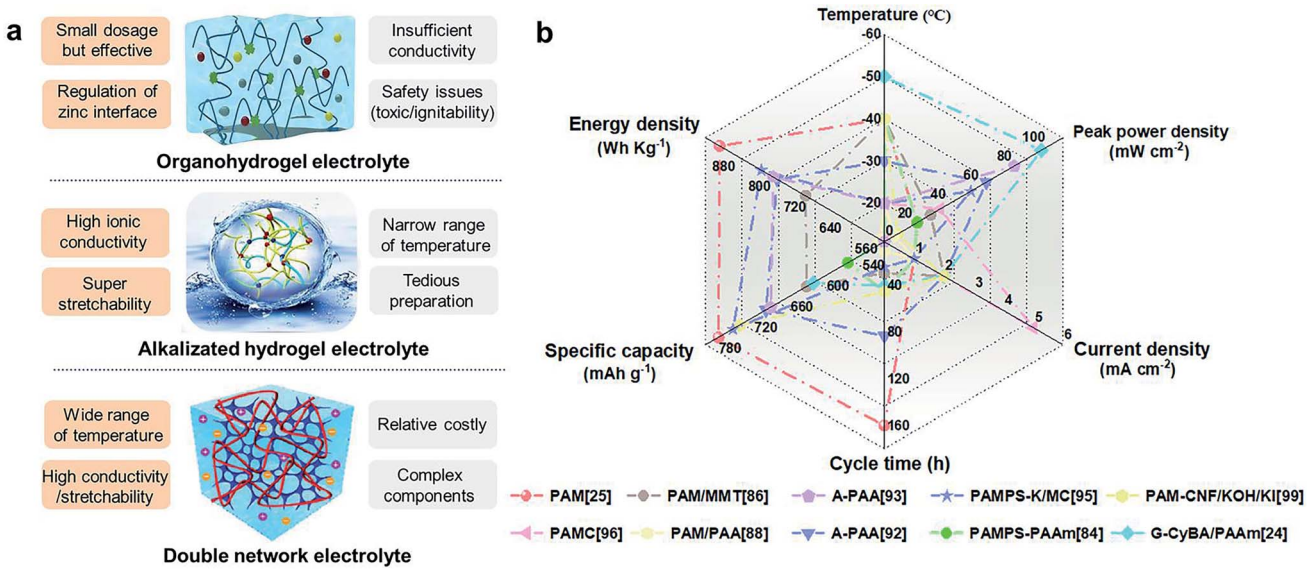

Fig. 11 (a) The comparison of the three design strategies for low-temperature resistant GPEs. Orange for pros and grey for cons. Reproduced with permission from ref. 92. Copyright 2020, Wiley. Reproduced with permission from ref. 24. Copyright 2021, Elsevier. (b) The performance of previously reported ZABs with low-temperature resistant hydrogels.

Table 1 Design of GPEs for low-temperature ZABs

Design strategy	GPEs' performance			ZABs' performance						Ref.
	Types	Elongation at 25 °C	Water retention at 25 °C	T (°C)	Ionic conductivity (mS cm^{-1})	Maximum power density (mW cm^{-2})	Specific capacity (mAh g^{-1})	Energy density (W h kg^{-1})	Cycle time (h) @current density (mA cm^{-2})	
Addition of organic solvent	PAM (DMSO)	620% at 0.04 Mpa	87.2% at 168 h	−60	0.087	—	—	—	300@0.5 100@1.0	25
				−40	0.4	21.9	778.4	918.5	160@1.0	
	PAM/MMT (DMSO)	—	—	−20	80.7	81	—	—	—	88
				−40	27.1	30	631	725	29@2.0	
	PAMPS-PAAm (DMSO)	370% at 220 kpa	64.2% at 40 h	−40	17.2	21.8	562	523.4	45@1	86
	PVA (EG)	—	—		—	—	—	—	—	23
	PAM/PAA (Gly)	500% at 110 kpa	19.1% at 48 h	−20	3.6	8.2	506.2	556.8	10@1	90
Alkalization	A-PAA	550% at 68 kpa	—	−30	90	63.6	699	789	83.3@2.0	94
		600% at 80 kpa	60% at 240 h	−20	199	80.5	691	798	—	95
Dual-network	G-CyBA/PAAm	1650% at 37 kpa	99% at 12 h	−50	252.2	97	620	—	40@2	24
	PAMC	700%	72% at 144 h	−20	96.3	35.8	—	—	3.5@5	98
	PAM-CNF/KOH/KI	319% at 16.3 kpa	86% at 12 h	−40	223	10	743	—	45@2	101
	PAMPS-K/MC	140% at 45 kpa	—	−20	18.1	54.2	754.2	824.6	24@1	97

mechanical strength and flexibility of DN hydrogels. The PAMPS-K/MC immersed in highly concentrated KOH solution displayed good freezing resistance, maintaining an ionic conductivity of 18.1 mS cm^{-1} at −20 °C. The specific capacities of the assembled DN hydrogel-based ZABs were essentially unabated when the temperature decreased from room temperature to 0 and −20 °C (Fig. 10c). Miao *et al.*[98] introduced cellulose into PAM to obtain a highly flexible DN electrolyte (PAMC). The PAMC could be easily stretched to 7 times its length without breaking and the water retention rate was still 72% after 144 h at room temperature. When PAMC was applied to ZABs at −20 °C, a maximum power density of 35.8 mW cm^{-2} and a stable cycle of 3.5 h were demonstrated. Notably, the absorption of high-concentration alkaline electrolyte and the synergistic interactions between polar groups played an important role in lowering the freezing point of DN GPEs.

Electrolyte additives could play a considerable role in modulating the charge/discharge behavior of ZABs.[99] For instance, Cheng and colleagues[100] suggested that the KI-containing ZABs undergoing the IO^{3-}/I^- mechanism had a much lower thermodynamic barrier than the batteries with the O_2/OH^- reaction happening at the air cathode, benefitting the reduction of charge voltage. Thus, Wei *et al.*[101] reported a DN hydrogel electrolytes consisting of PAM and cellulose nanofibers with KOH/KI solution (PAM-CNF/KOH/KI). The lowest I_{3295}/I_{3470} (strong O–H in tetrahedra/weak O–H in incomplete tetrahedra) of 0.82 towards PAM-CNF/KOH/KI indicated that the ion–water interactions significantly weakened the hydrogen bonds between H_2O molecules (Fig. 10d). Due to the formed hydrogen bonds between polymer–water and the disrupted hydrogen bonding structure of free H_2O molecules by ionic hydration, the freezing point of GPEs was significantly reduced. The electrical conductivity of hydrogels remained stable during repeated cooling–heating–cooling cycles, implying their excellent stability to temperature changes (Fig. 10e). Therefore, PAM-CNF/KOH/KI-based ZABs exhibited great electrochemical performances even at −40 °C (Fig. 10f). The maximum power density of 10 mW cm^{-2} and a stable discharge platform at 10 mA cm^{-2} were presented. The above research studies illustrated the significance of the DN electrolyte modification in reducing freezing temperature and improving mechanical properties, which provided the reference for exploring suitable polymer systems in cold environments.

4. Conclusions and outlook

This review summarizes the up-to-date advances in low-temperature resistant GPEs in ZABs. As the ''blood'' of flexible ZABs, multifunctional GPEs significantly affect battery performance through the modulation of mass transfer and interfacial behavior. The above-mentioned three strategies provide mainstream design directions for the development of low-temperature resistant GPEs. Their pros and cons are summarized in Fig. 11a. In order to meet the demand for low-temperature and flexible application scenarios, the continuous optimization of cost, ionic conductivity, flexibility, temperature adaptability, and environmental friendliness should be carried out. Based on

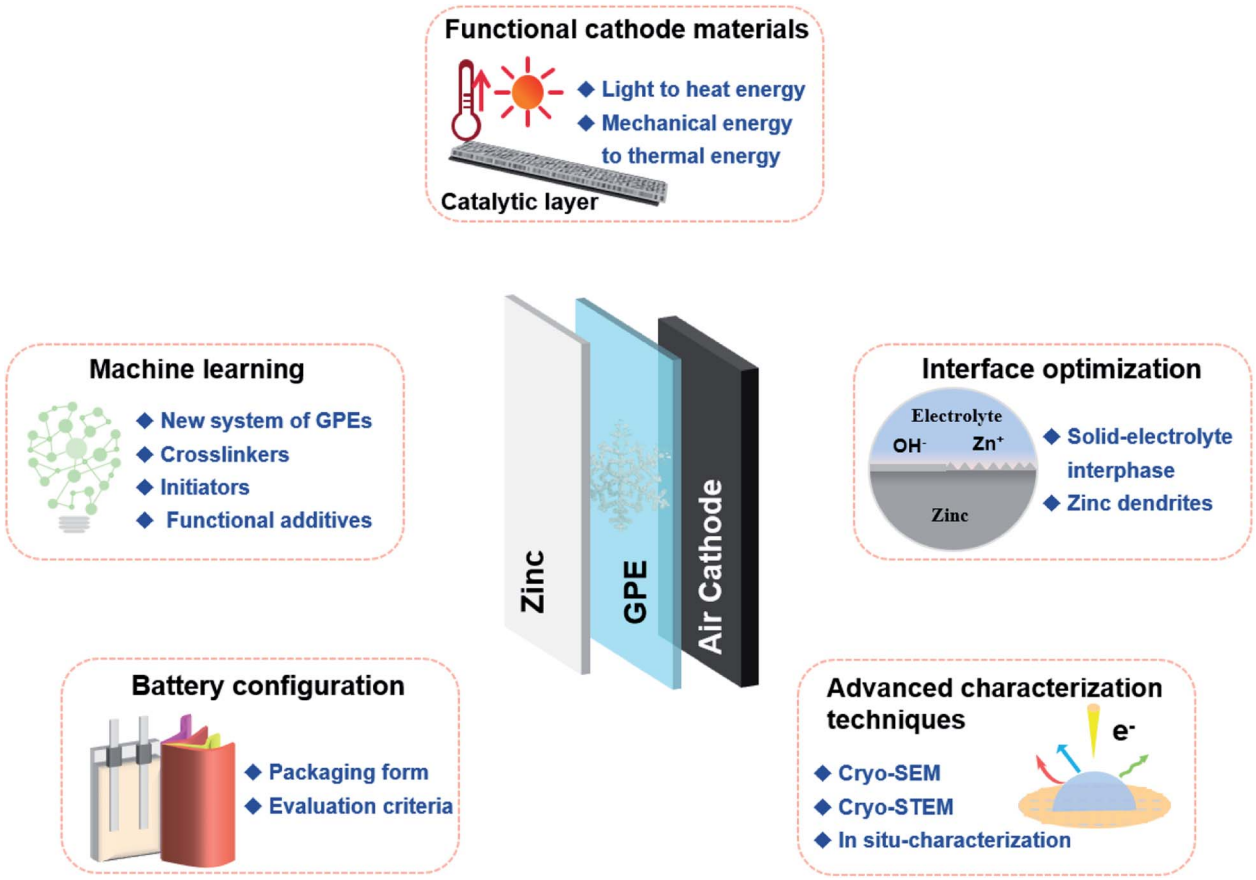

Fig. 12 Prospects of low-temperature resistant GPEs towards ZABs.

antifreeze GPEs, the performances of ZABs at low temperatures are concluded in Fig. 11b and Table 1. The decreased current densities during charge/discharge at low temperatures were observed, indicating slow cycling processes and weak rate performances. Furthermore, the power density, specific capacity and cycle life of GPE based ZABs at low temperatures were severely degraded compared to those at room temperatures. Hence, the ion transport, low-temperature tolerance, and the GPEs/electrodes interface stability should be paid attention. In addition, to evaluate the low-temperature performance of GPEs and the corresponding ZABs, the detailed characterization and in-depth mechanism of antifreezing electrolytes are needed to reveal the structure–performance relationships. The systematic and comprehensive testing criteria should also be established. Based on the above discussions, some challenges and perspectives are put forward, hoping to push the development of low-temperature ZABs out of the stage of laboratory exploration (Fig. 12).

(1) New GPEs systems and various functional material additives for low-temperature applications remain to be developed. At present, the variety of monomers suitable for GPEs is limited. There is much room to investigate initiators and crosslinkers in the polymerization process to improve the physicochemical properties of GPEs. At the same time, additives can be added to increase the electrical conductivity and promote the decomposition/deposition of zinc to inhibit the growth of zinc dendrites. Of course, proper modification of the electrolyte should ensure a good match at GPEs/electrode interfaces to achieve long-term stability. It is worth noting that with the rapid development of machine learning-enhanced high-throughput experiments,[102] a large number of potential candidate compounds and inorganic fillers can be screened from the materials database to achieve GPEs with coupled low-temperature resistance and high conductivity. The successful combination of simulation and experiment will promote the research of GPEs with low cost, high performance and a wide-temperature domain.

(2) The interfacial film between GPEs and the zinc anode is critical to low-temperature performance. Since different GPEs produce specific interfaces with the zinc anode, the specific reaction properties need to be studied systematically. Meanwhile, the growth of zinc dendrites on the anode surface will seriously damage the output performance and service life of batteries. In addition to electrolyte modification, zinc dendrites could be inhibited to some extent by designing a protective coating, which is beneficial to eliminate the “tip effect” and improve the cycling stability.[103] Further in-depth research should be carried out to reveal the failure mechanism of ZABs at low temperature.

(3) Although the oxygen catalysis performance of air electrodes is insensitive to low temperature, functional modification of air electrodes is expected to improve the interfacial

characteristics and ion transport behavior of adjacent GPEs. For example, the additives in the catalyst layer with the ability to convert light energy to thermal energy will increase the temperature inside the ZABs, thereby enhancing low-temperature tolerance.[104] Considering the possible mechanical deformation of flexible ZABs during operation, the conversion of mechanical energy to thermal energy is another way to improve low-temperature resistance. Notably, the excellent conductivity and gas transport capability should be maintained when air electrodes are functionally modified.[105]

(4) In order to better explain the mechanism of attenuated battery performance, it is necessary to explore more reliable and advanced characterization techniques to analyze ion diffusion and complex interface evolution at low temperature, such as cryo-SEM, cryo-STEM, *etc.*[106] Furthermore, the non-destructive and highly quantitative *in situ* detection methods are expected to reveal the electrochemical reactions at low temperature or under stress and strain conditions. However, the currently existing flexible battery structures pose great challenges to the construction of *in situ* characterization devices. The coupling of battery, environment, stress application devices and detection systems, *etc.*, needs to be comprehensively considered.

(5) The configuration of flexible ZABs needs to be further optimized. At present, the configuration of ZABs is basically the traditional battery template. However, wearable devices require high bending, warping and even stretching performance. And the packaging forms of flexible ZABs should also suit harsh environments (desiccation, high humidity, high temperatures, high pressure, *etc.*). Among them, the integrated micro-batteries with self-standing electrodes was noted for they are well-suited to wearable devices.[107] Furthermore, standardized criteria and tests should be established not only for mechanical properties of GPEs and electrodes (such as bending times, compressive ability, tensile properties, *etc.*), but also for the flexibility of ZABs.

Conflicts of interest

There are no conflicts of interest to declare.

Acknowledgements

This work was financially supported by the State Key Laboratory of Powder Metallurgy, Central South University.

References

1 H. Z. Dou, M. Xu, Y. Zheng, Z. Q. Li, G. B. Wen, Z. Zhang, L. X. Yang, Q. Y. Ma, A. P. Yu, D. Luo, X. Wang and Z. W. Chen, *Adv. Mater.*, 2022, **34**, 2110585.
2 S. Wang, J. Xu, W. Wang, G. J. N. Wang, R. Rastak, F. Molina-Lopez, J. W. Chung, S. Niu, V. R. Feig, J. Lopez, T. Lei, S. K. Kwon, Y. Kim, A. M. Foudeh, A. Ehrlich, A. Gasperini, Y. Yun, B. Murmann, J. B. H. Tok and Z. Bao, *Nature*, 2018, **555**, 83–88.
3 S. Y. Zhao, D. W. Xia, M. H. Li, D. Y. Cheng, K. L. Wang, Y. S. Meng, Z. Chen and J. Bae, *ACS Appl. Mater. Interfaces*, 2021, **13**, 12033–12041.
4 Y. C. Wang, L. Xu, L. S. Zhan, P. Y. Yang, S. H. Tang, M. J. Liu, X. Zhao, Y. Xiong, Z. Y. Chen and Y. P. Lei, *Nano Energy*, 2022, **92**, 106780.
5 M. F. Chen, W. J. Zhou, A. R. Wang, A. X. Huang, J. Z. Chen, J. L. Xu and C. P. Wong, *J. Mater. Chem. A*, 2020, **8**, 6828–6841.
6 Y. X. Zuo, Y. Yu, C. C. Zuo, C. L. Ning, H. Liu, Z. Q. Gu, Q. Q. Cao and C. M. Shen, *Energies*, 2019, **12**, 612.
7 Y. Ma, A. Sumboja, W. Zang, S. Yin, S. Wang, S. J. Pennycook, Z. K. Kou, Z. L. Liu, X. Li and J. Wang, *ACS Appl. Mater. Interfaces*, 2019, **11**, 1988–1995.
8 B. Sun, K. Kretschmer, X. Xie, P. Munroe, Z. Peng and G. Wang, *Adv. Mater.*, 2017, **29**, 1606816.
9 H. S. Hirsh, Y. X. Li, D. H. S. Tan, M. H. Zhang, E. Y. Zhao and Y. S. Meng, *Adv. Energy Mater.*, 2020, **10**, 2001274.
10 J. Fu, Z. P. Cano, M. G. Park, A. P. Yu, M. Fowler and Z. W. Chen, *Adv. Mater.*, 2017, **29**, 1604685.
11 M. A. Rahman, X. Wang and C. Wen, *J. Electrochem. Soc.*, 2013, **160**, A1759.
12 F. X. Wu and G. Yushin, *Energy Environ. Sci.*, 2017, **10**, 435–459.
13 J. S. Lee, S. T. Kim, R. Cao, N. S. Choi, M. Liu, K. T. Lee and J. Cho, *Adv. Energy Mater.*, 2011, **1**, 2.
14 M. F. Sanad, A. R. P. Santiago, S. A. Tolba, M. A. Ahsan, O. F. Delgado, M. S. Adly, E. M. Hashem, M. M. Abodouh, M. S. El-Shall, S. T. Sreenivasan, N. K. Allam and L. Echegoyen, *J. Am. Chem. Soc.*, 2021, **143**, 4064–4073.
15 A. Smee, *Philos. Mag.*, 1840, **16**, 315–321.
16 L. Maiche, *French Pat*, 1878, 127069.
17 P. Gu, M. B. Zheng, Q. X. Zhao, X. Xiao, H. G. Xue and H. Pang, *J. Mater. Chem. A*, 2017, **5**, 7651–7666.
18 A. R. Mainar, L. C. Colmenares, J. A. Blázquez and I. Urdampilleta, *Int. J. Energy Res.*, 2018, **42**, 903–918.
19 J. Fu, D. U. Lee, F. M. Hassan, L. Yang, Z. Y. Bai, M. G. Park and Z. W. Chen, *Adv. Mater.*, 2015, **27**, 5617–5622.
20 J. Park, M. Park, G. Nam, J. S. Lee and J. Cho, *Adv. Mater.*, 2015, **27**, 1396–1401.
21 L. An, B. L. Huang, Y. Zhang, R. Wang, N. Zhang, T. Y. Dai, P. X. Xi and C. H. Yan, *Angew. Chem., Int. Ed.*, 2019, **58**, 9459–9463.
22 K. Tang, C. Z. Yuan, Y. Xiong, H. B. Hu and M. Z. Wu, *Appl. Catal., B*, 2020, **260**, 118209.
23 J. Yin, J. Jin, H. B. Liu, B. L. Huang, M. Lu, J. Y. Li, H. W. Liu, H. Zhang, Y. Peng, P. X. Xi and C. H. Yan, *Adv. Mater.*, 2020, **32**, 2001651.
24 C. N. Gu, X. Q. Xie, Y. J. Liang, J. J. Li, H. Wang, K. F. Wang, J. P. Liu, M. K. Wang, Y. F. Zhang, M. X. Li, H. J. Kong and C. S. Liu, *Energy Environ. Sci.*, 2021, **14**, 4451–4462.
25 Q. C. Wang, Q. G. Feng, Y. P. Lei, S. H. Tang, L. Xu, Y. Xiong, G. Z. Fang, Y. C. Wang, P. Y. Yang, J. J. Liu, W. Liu and X. Xiong, *Nat. Commun.*, 2022, DOI: 10.1038/s41467-022-31383-4.
26 J. W. Hu, X. B. Cai, J. Wu, C. C. Xin, J. Y. Guo, Z. R. Liu, J. Z. Wei, X. S. Cheng, C. Hao, H. P. Dong, G. F. Zhang,

N. Wang, Y. P. Lei, W. Liu and Y. T. Shi, *Chem. Eng. J.*, 2022, **430**, 133105.
27 W. Sun, F. Wang, B. Zhang, M. Y. Zhang, V. Küpers, X. Ji, C. Theile, P. Bieker, K. Xu, C. S. Wang and M. Winter, *Science*, 2021, **371**, 46–51.
28 L. J. Li and A. Manthiram, *Adv. Energy Mater.*, 2016, **6**, 1502054.
29 M. Kar, B. Winther-Jensen, M. Armand, T. J. Simons, O. Winther-Jensen, M. Forsyth and D. R. MacFarlane, *Electrochim. Acta*, 2016, **188**, 461–471.
30 X. R. Liu, X. Y. Fan, B. Liu, J. Ding, Y. D. Deng, X. P. Han, C. Zhong and W. B. Hu, *Adv. Mater.*, 2021, **33**, 2006461.
31 X. L. Xu, S. Wang, S. Q. Guo, K. S. Hui, J. M. Ma, D. A. Dinh, K. N. Hui, H. Wang, L. P. Zhang and G. W. Zhou, *Adv. Powder Mater.*, 2022, **1**, 100027.
32 J. Sun, N. K. Guo, T. S. Song, Y. R. Hao, J. W. Sun, H. Xue and Q. Wang, *Adv. Powder Mater.*, 2022, **1**, 100023.
33 P. Tan, B. Chen and H. R. Xu, *Energy Environ. Sci.*, 2017, **10**, 2056–2080.
34 L. T. Ma, S. M. Chen, D. H. Wang, Q. Yang, F. N. Mo, G. J. Liang, N. Li, H. Y. Zhang, J. A. Zapien and C. Y. Zhi, *Adv. Energy Mater.*, 2019, **9**, 1803046.
35 J. Fu, J. Zhang, X. Song, H. Zarrin, X. Tian, J. Qiao, L. Rasen, K. Li and Z. Chen, *Energy Environ. Sci.*, 2016, **9**, 663–670.
36 J. Fu, F. M. Hassan, C. Zhong, J. Lu, H. Liu, A. Yu and Z. Chen, *Adv. Mater.*, 2017, **29**, 1702526.
37 Y. Y. Zuo, K. L. Wang, M. H. Wei, S. Y. Zhao, P. F. Zhang and P. C. Pei, *Cell Rep. Phys. Sci.*, 2022, **3**, 100687.
38 M. J. Wu, G. X. Zhang, L. Du, D. C. Yang, H. M. Yang and S. H. Sun, *Small Methods*, 2021, **5**, 2000868.
39 X. Gong, Q. Yang, C. Zhi and P. S. Lee, *Adv. Energy Mater.*, 2021, **11**, 2003308.
40 T. Liu, J. Mou, Z. Wu, C. Lv, J. Huang and M. Liu, *Adv. Funct. Mater.*, 2020, **30**, 2003407.
41 Z. Cao, H. Hu, M. Wu, K. Tang and T. Jiang, *J. Mater. Chem. A*, 2019, **7**, 17581–17593.
42 H. Miao, B. Chen, S. Li, X. Wu, Q. Wang, C. Zhang, Z. Sun and H. Li, *J. Power Sources*, 2020, **450**, 227653.
43 M. Z. Chen, Y. Y. Zhang, G. C. Xing, S.-L. Chou and Y. X. Tang, *Energy Environ. Sci.*, 2021, **14**, 3323–3351.
44 S. H. Li, H. Y. Pan, Y. T. Wang and J. Q. Sun, *J. Mater. Chem. A*, 2020, **8**, 3667–3675.
45 Z. X. Liu, X. B. Luo, L. P. Qin, G. Z. Fang and S. Q. Liang, *Adv. Powder Mater.*, 2022, **1**, 100011.
46 C. X. Zhao, J. N. Liu, N. Yao, J. Wang, D. Ren, X. Chen, B. Q. Li and Q. Zhang, *Angew. Chem., Int. Ed.*, 2021, **60**, 15281–15285.
47 Z. Chen, X. L. Li, D. H. Wang, Q. Yang, L. T. Ma, Z. D. Huang, G. J. Liang, A. Chen, Y. Guo, B. B. Dong, X. Y. Huang, C. Yang and C. Y. Zhi, *Energy Environ. Sci.*, 2021, **14**, 3492–3501.
48 C. Lu and X. Chen, *Nano Lett.*, 2020, **20**, 1907–1914.
49 X. T. Jin, L. Song, C. L. Dai, H. Y. Ma, Y. K. Xiao, X. Q. Zhang, Y. Y. Han, X. Y. Li, J. T. Zhang, Y. Zhao, Z. P. Zhang, L. Duan and L. T. Qu, *Energy Storage Mater.*, 2022, **44**, 517–526.
50 F. Mo, G. Liang, Q. Meng, Z. Liu, H. Li, J. Fan and C. Zhi, *Energy Environ. Sci.*, 2019, **12**, 706–715.
51 F. Mo, G. Liang, D. Wang, Z. Tang, H. Li and C. Zhi, *EcoMat*, 2019, **1**, e12008.
52 X. J. Sui, H. S. Guo, P. G. Chen, Y. N. Zhu, C. Y. Wen, Y. H. Gao, J. Yang, X. Y. Zhang and L. Zhang, *Adv. Funct. Mater.*, 2020, **30**, 1907986.
53 M. F. Chen, J. Z. Chen, W. J. Zhou, X. Han, Y. G. Yao and C. P. Wong, *Adv. Mater.*, 2021, **33**, 2007559.
54 J. Mindemark, M. J. Lacey, T. Bowden and D. Brandell, *Prog. Polym. Sci.*, 2018, **81**, 114–143.
55 Y. T. Wei, Y. C. Shi, Y. Chen, C. H. Xiao and S. J. Ding, *J. Mater. Chem. A*, 2021, **9**, 4415–4453.
56 F. Santos, J. P. Tafur, J. Abad and A. J. F. Romero, *J. Electroanal. Chem.*, 2019, **850**, 113380.
57 Y. H. Ye, Y. F. Zhang, Y. Chen, X. S. Han and F. Jiang, *Adv. Funct. Mater.*, 2020, **30**, 2003430.
58 Q. F. Rong, W. W. Lei, J. Huang and M. J. Liu, *Adv. Energy Mater.*, 2018, **8**, 1801967.
59 G. W. Shao, R. Yu, X. Zhang, X. Chen, F. L. He, X. Zhao, N. L. Chen, M. D. Ye and X. Y. Liu, *Adv. Funct. Mater.*, 2020, **30**, 2003153.
60 A. Lewandowski, K. Skorupska and J. Malinska, *Ionics*, 2000, **133**, 265–271.
61 L. Yang, L. Shi, D. Wang, Y. L. Lv and D. P. Cao, *Nano Energy*, 2018, **50**, 691–698.
62 Q. S. Nian, T. J. Sun, S. Liu, H. H. Du, X. D. Ren and Z. L. Tao, *Chem. Eng. J.*, 2021, **423**, 130253.
63 H. Y. Lu, J. S. Hu, L. T. Wang, J. Z. Li, X. Ma, Z. C. Zhu, H. Q. Li, Y. J. Zhao, Y. J. Li, J. X. Zhao and B. G. Xu, *Adv. Funct. Mater.*, 2022, **32**, 2112540.
64 H. W. Kim, J. M. Lim, H. J. Lee, S. W. Eom, Y. T. Hong and S.-Y. Lee, *J. Mater. Chem. A*, 2016, **4**, 3711–3720.
65 Y. Zhong, Z. Pan, X. Wang, J. Yang, Y. Qiu, S. Xu, Y. Lu, Q. Huang and W. Li, *Adv. Sci.*, 2019, **6**, 1802243.
66 C. X. Zheng, K. Y. Lu, Y. Lu, S. L. Zhu, Y. Y. Yue, X. W. Xu, C. T. Mei, H. N. Xiao, Q. L. Wu and J. Q. Han, *Carbohydr. Polym.*, 2020, **250**, 116905.
67 Q. Wang, H. Miao, S. Sun, Y. Xue and Z. Liu, *Chem.–Eur. J.*, 2018, **24**, 14816–14823.
68 C. Iwakura, N. Furukawa, T. Ohnishi, K. Sakamoto, S. Nohara and H. Inoue, *Electrochemistry*, 2001, **69**, 659–663.
69 Y. Huang, Z. Li, Z. X. Pei, Z. X. Liu, H. F. Li, M. S. Zhu, J. Fan, Q. B. Dai, M. D. Zhang, L. M. Dai and C. Y. Zhi, *Adv. Energy Mater.*, 2018, **8**, 1802288.
70 H. Wang, J. Liu, J. Q. Wang, M. M. Hu, Y. P. Feng, P. P. Wang, Y. Y. Wang, N. Y. Nie, J. H. Zhang, H. Chen, Q. H. Yuan, J. W. Wu and Y. Huang, *ACS Appl. Mater. Interfaces*, 2019, **11**, 49–55.
71 L. Sartore, S. Pandini, F. Baldi, F. Bignotti and L. D. Landro, *J. Appl. Polym. Sci.*, 2017, **134**, 45655.
72 T. T. Wei, Y. K. Ren, Z. Q. Li, X. X. Zhang, D. H. Ji and L. H. Hu, *Chem. Eng. J.*, 2022, **434**, 134646.
73 J. Zhang, L. D Zeng, Z. W. Qiao, J. Wang, X. C. Jiang, Y. S. Zhang and H. H. Yang, *ACS Appl. Mater. Interfaces*, 2020, **12**, 30247–30258.
74 L. Ma, S. Chen, Z. Pei, Y. Huang, G. Liang, F. Mo, Q. Yang, J. Su, Y. Gao, J. A. Zapien and C. Zhi, *ACS Nano*, 2018, **12**, 1949–1958.

75 X. F. Zhang, X. F. Ma and T. Hou, *Angew. Chem., Int. Ed.*, 2019, **58**, 7366–7370.
76 Z. G. Zhao, K. J. Zhang, Y. X. Liu, J. J. Zhou and M. J. Liu, *Adv. Mater.*, 2017, **29**, 1701695.
77 W. X. Shang, W. T. Yu, Y. Y. Ma, Y. He, Z. X. Zhao, M. Ni, H. Zhao and P. Tan, *Adv. Mater. Interfaces*, 2021, **8**, 2101256.
78 Z. F. Wang, H. F. Li, Z. J. Tang, Z. X. Liu, Z. H. Ruan, L. T. Ma, Q. Yang, D. H. Wang and C. Y. Zhi, *Adv. Funct. Mater.*, 2018, **28**, 1804560.
79 S. Y. Zhao, Y. Y. Zuo, T. Liu, S. Zhai, Y. W. Dai, Z. J. Guo, Y. Wang, Q. J. He, L. C. Xia, C. Y. Zhi, J. Bae, K. L. Wang and M. Ni, *Adv. Energy Mater.*, 2021, **11**, 2101749.
80 S. W. Huang, L. Hou, T. Y. Li, Y. C. Jiao and P. Y. Wu, *Adv. Mater.*, 2022, **34**, 2110140.
81 B. Y. Zhang, L. P. Qin, Y. Fang, Y. Z. Chai, X. S. Xie, B. G. Lu, S. Q. Liang and J. Zhou, *Sci. Bull.*, 2022, **67**, 955–962.
82 L. H. Li, H. Chen, E. He, L. Wang, T. T. Ye, J. Lu, Y. D. Jiao, J. C. Wang, R. Gao, H. S. Peng and Y. Zhang, *Angew. Chem., Int. Ed.*, 2021, **60**, 15317–15322.
83 L. Chen, Y. P. Wang, X. Zhao, Y. C. Wang, Q. Li, Q. C. Wang, Y. G. Tang and Y. P. Lei, *J. Mater. Sci. Technol.*, 2022, **110**, 128–135.
84 Q. Li, Y. C. Wang, J. Zeng, Q. M. Wu, Q. C. Wang, L. Sun, L. Xu, T. Ye, X. Zhao, L. Chen, Z. Y. Chen, L. M. Chen and Y. P. Lei, *Chinese Chem. Lett.*, 2021, **32**, 3355–3358.
85 F. Q. Cao, B. H. Wu, T. Y. Li, S. T. Sun, Y. C. Jiao and P. Y. Wu, *Nano Res.*, 2022, **15**, 2030–2039.
86 D. Q. Jiang, H. Y. Wang, S. Wu, X. Y. Sun and J. Li, *Small Methods*, 2021, **6**, 2101043.
87 Y. Ma, L. B. Li, G. X. Gao, X. Y. Yang and Y. You, *Electrochim. Acta*, 2016, **187**, 535–542.
88 T. T. Cui, Y. P. Wang, T. Ye, J. Wu, Z. Q. Chen, J. Li, Y. P. Lei, D. S. Wang and Y. D. Li, *Angew. Chem., Int. Ed.*, 2022, **61**, e202115219.
89 E. Cevik, S. T. Gunday, A. Bozkurt, R. Amine and K. Amine, *J. Power Sources*, 2020, **474**, 228544.
90 R. Chen, X. B. Xu, S. Y. Peng, J. M. Chen, D. F. Yu, C. H. Xiao, Y. L. Li, Y. T. Chen, X. F. Hu, M. J. Liu, H. Yang, I. Wyman and X. Wu, *ACS Sustainable Chem. Eng.*, 2020, **8**, 11501–11511.
91 Z. Z. Liu, J. M. Zhang, J. Liu, Y. J. Long, L. M. Fang, Q. W. Wang and T. Liu, *J. Mater. Chem. A*, 2020, **8**, 6219–6228.
92 L. Han, K. Liu, M. Wang, K. Wang, L. Fang, H. Chen, J. Zhou and X. Lu, *Adv. Funct. Mater.*, 2018, **28**, 1704195.
93 Z. Lin, C. Qiang and X. Kun, *Prog. Chem.*, 2014, **26**, 1032–1038.
94 Z. X. Pei, Z. W. Yuan, C. J. Wang, S. L. Zhao, J. Y. Fei, L. Wei, J. S. Chen, C. Wang, Ro. J. Qi, Z. W. Liu and Y. Chen, *Angew. Chem., Int. Ed.*, 2020, **59**, 4793–4799.
95 Z. X. Pei, L. Y. Ding, C. Wang, Q. Q. Meng, Z. W. Yuan, Z. Zhou, S. L. Zhao and Y. Chen, *Energy Environ. Sci.*, 2021, **14**, 4926–4935.
96 J. Cong, Z. W. Fan, S. S. Pan, J. Tian, W. Z. Lian, S. Li, S. J. Wang, D. C. Zheng, C. G. Miao, W. P. Ding, T. L. Sun and T. Z. Luo, *ACS Appl. Mater. Interfaces*, 2021, **13**, 34942–34953.
97 N. Sun, F. Lu, Y. Yu, L. Su, X. P. Gao and L. Q. Zheng, *ACS Appl. Mater. Interfaces*, 2020, **12**, 11778–11788.
98 B. Chen, H. Miao, M. M. Yin, R. G. Hu, L. Xia, C. F. Zhang and J. L. Yuan, *Chem. Eng. J.*, 2021, **417**, 129179.
99 J. Cao, D. D. Zhang, R. Chanajaree, Y. L. Yue, Z. Y. Zeng, X. Y. Zhang and J. Q. Qin, *Adv. Powder Mater.*, 2022, **1**, 100007.
100 Z. H. Song, J. Ding, B. Liu, X. R. Liu, X. P. Han, Y. D. Deng, W. B. Hu and C. Zhong, *Adv. Mater.*, 2020, **32**, 1908127.
101 Y. N. Zhang, H. L. Qin, M. Alfred, H. Z. Ke, Y. B. Cai, Q. Q. Wang, F. L. Huang, B. Liu, P. F. Lv and Q. F. Wei, *Energy Storage Mater.*, 2021, **42**, 88–96.
102 H. Y. Jing, P. Zhu, X. B. Zheng, Z. D. Zhang, D. S. Wang and Y. D. Li, *Adv. Powder Mater.*, 2022, **1**, 100013.
103 J. X. Zheng, Z. H. Huang, Y. Zeng, W. Q. Liu, B. B. Wei, Z. B. Qi, Z. H. Wang, C. Xia and H. F. Liang, *Nano Lett.*, 2022, **22**, 1017–1023.
104 H. C. Song, S. Wang, X. Y. Song, J. Wang, K. Z. Jiang, S. H. Huang, M. Han, J. Xu, P. He, K. J. Chen and H. S. Zhou, *Energy Environ. Sci.*, 2020, **13**, 1205–1211.
105 Y. C. Wang, Y. Liu, W. Liu, J. Wu, Q. Li, Q. G. Feng, Z. Y. Chen, X. Xiong, D. S. Wang and Y. P. Lei, *Energy Environ. Sci.*, 2020, **13**, 4609–4624.
106 Z. W. Zhang, Y. Z. Li, R. Xu, W. J. Zhou, Y. B. Li, S. T. Oyakhire, Y. C. Wu, J. W. Xu, H. S. Wang, Z. Yu, D. T. Boyle, W. Huang, Y. Ye, H. Chen, J. Wan, Z. N. Bao, W. Chiu and Y. Cui, *Science*, 2022, **375**, 66–70.
107 Y. P. Lei, Q. C. Wang, S. J. Peng, S. Ramakrishna, D. Zhang and K. C. Zhou, *Adv. Energy Mater.*, 2020, **10**, 1902115.